Proposal of a Mask and Its Performance Analysis with CFD for an Enhanced Aerodynamic Geometry That Facilitates Filtering and Breathing against COVID-19

Boris Miguel López-Rebollar [ID], Abad Posadas-Bejarano, Daury García-Pulido, Adrián Torres-Maya and Carlos Díaz-Delgado *[ID]

Instituto Interamericano de Tecnología y Ciencias del Agua, Universidad Autónoma del Estado de México, Toluca 50200, Mexico; bmlopezr@uaemex.mx (B.M.L.-R.); aposadasb@uaemex.mx (A.P.-B.); dgarciap@uaemex.mx (D.G.-P.); atorresm@uaemex.mx (A.T.-M.)
* Correspondence: cdiazd@uaemex.mx

Abstract: As a result of the recent events associated with the SARS-CoV-2 around the world, there has been a need for research to strengthen health care. The use of masks or respirators has been an effective measure, reducing the risk of contagion caused by the spread of the virus in public places. Currently, there are masks that retain up to 99% of particles >0.3 microns; however, they lack an airtight seal with the face, leading to discomfort and poor protection in conditions without social distancing and areas without ventilation. The device proposed in this study includes a geometric design of static valves with convergent spirals and interior baffles that promotes enhanced aerodynamics with bidirectional flow. According to the analysis and CFD simulation of the proposed reusable, washable, and economic mask and valve system for breathing, coughing, and sneezing events, enhanced air exchange could be maintained, facilitating a higher inhalation flow through the side of the mask (62%) and a higher exhalation through the front of the mask (74%), thereby avoiding the recirculation of the flow to the interior of the mask. The inclusion of filters with KN95 characteristics in the inlets and outlets maintains velocities below 10 cm/s, reducing the probability of infection.

Keywords: flow simulation; porous media; geometric design; turbulence flow; COVID-19

1. Introduction

In March 2020, the World Health Organization (WHO) [1] declared a state of global pandemic derived from COVID-19 disease. In the United States of America, there was an increase from 300 to 1.5 million cases of the contagion in a period of 2 months, while the number of deaths increased from 8000 to 100,000 in the same period [2]. This situation, as in many countries, was caused by the rapid spread of the virus through people and in crowded places where there was no social distancing. In North American countries, during March 2020, cases of infection and deaths caused by the SARS-CoV-2 virus were reported, where the general probability of survival was 87.7% from day 24 of infection [3]. Over time, it was observed that the mortality rate increased in the elderly and was associated with deaths from pneumopathies and neurological and cardiovascular deaths. This situation subsequently occurred in several countries and in other continents where the spread of the COVID-19 disease existed.

In Mexico, the number of infected cases of COVID-19 in May 2020 was 23,471, which increased to approximately 200,000 a month later [4]. The increase in deaths and infections was mainly due to the accelerated reopening of the economy and the limited control in the restrictions of confinement and social distancing. The total number of confirmed deaths from COVID-19 was 221,200 from January 2020 to May 2021, and the total number of confirmed cases of the contagion was 2,576,029 during the same period, which represents approximately 2% of the total country population [5].

Worldwide, there were 167,011,807 confirmed cases of the contagion and 3,472,068 deaths associated with COVID-19 until May 2021 according to data published on the official website of the World Health Organization (WHO) [1], and the North American continent is ranked first as the region with the highest number of infections and deaths. As a result, the WHO has issued several recommendations to continue mitigating the rapid spread of COVID-19, mainly in developing countries. Some of the recommendations focus on the use of face masks or respirators, as well as promoting social distancing in public spaces.

Currently, there are several studies where it is highlighted that the main transmission of COVID-19 is carried out among people who do not present any symptoms. In addition, the main means of contagion in these cases is through contact with dirty or contaminated hands and surfaces [6]. On the other hand, it has been shown that the SARS-CoV-2 virus remains active up to 1 h after its volatilization after a respiratory event, such as coughing or sneezing, a situation that does not occur with other viruses [7]. In the last decade, there has been an increase in the studies and research on the behavior of airborne dispersal and contagion of viral and bacterial diseases among humans, such as influenza virus subtype AH1N1 and the severe acute respiratory syndrome coronavirus 2 (SARS-CoV-2), which generates the disease known as COVID-19.

The transmission of diseases between humans is caused mainly through respiratory events, such as talking, eating, coughing, and sneezing [8–10]. Consequently, several studies have analyzed the dispersion and transport of particles to establish critical scenarios where it is necessary to maintain a minimum distance between people to avoid the spread of diseases; this concept has been called social distance [11]. In addition, confined public spaces with adequate ventilation play a very important role in reducing the risk of infection. As a result, several studies have focused on analyzing the relationship and interaction between social distance, ventilation rate, and the probability of infection [12].

Two of the main respiratory events that cause a greater risk of contagion through air transportation are coughing and sneezing. These events are considered violent and usually occur when an individual has a viral or bacterial disease. Coughing and sneezing generate the expulsion of particles with diameters <5–10 microns in the form of a cloud with an average exhalation velocity of 11.2 m/s and with falling velocities of the particles <3 mm/s [8,10].

Exhalation respiratory events, such as sneezing and coughing, have flow velocities of up to 50 m/s and 10 m/s, respectively, with particles of 60 and 100 microns in diameter expelled in these events travelling a distance up to 1–2 m before falling to the ground or evaporating [13]. Therefore, several studies have been carried out with the purpose of examining the distribution of ventilation and protection systems in public spaces, such as hospitals, to control airborne particles and minimize the dispersion of particles related to diseases that could be transmitted [9].

Based on the events that emerged in December 2019 around the contagion of the COVID-19 disease, the global need to use facial masks (made by different layer mallets or homemade clothes) or cone-shaped respirators (filtering facepiece respirators-FFR) with quality control that guarantees a retention of at least 95% of particles up to 0.3 microns (N95—United States NIOSH-42CFR84; FFP2—Europe EN 149-2001; KN95—China GB2626-2006) emerged to mitigate the spread of the virus between people. In this regard, Beesoon et al. [14] present a discussion about the effectiveness of masks, especially those made of textile materials. In their research, the authors highlight the ideal characteristics that a mask should have to guarantee the protection of the user. Among the main characteristics are: (a) a good filtering capacity for inhalation and exhalation events; (b) low resistance to respiration and gas exchange efficiency; (c) washable or reusable; and, finally, (d) comfortable use.

Other studies that analyze the effect of wind in open spaces also suggest the use of face masks to prevent and reduce the risk of contagion by the possible presence of airborne pathogens. This condition has generated a greater number of respiratory diseases, so it is desirable to use comfortable, safe, and efficient masks with good air exchange and the effective filtration of particles. Thus, the use of masks can be a feasible alternative

to mitigate the rapid contagion and transmission of diseases between individuals [15]. Xi et al. [16] studied the effects of wearing a surgical mask for inhalation events to evaluate the filtration and trajectories of virus-laden particles over the mask and respiratory tract. They found that masks can reduce the 10 microns particle penetration into the lungs regardless of the filtration efficiency of the mask. Another example is mentioned by Leonard et al. [17] where they found that the dispersion of characterized particles in a therapy room can be prevented using surgical masks with the presence of low velocities at the outlets of the mask. In fact, some research [18] recently found that suspended particulate matter with a diameter <2.5 microns (PM2.5), diameter <10 microns (PM10), as well as certain CO levels and temperatures are four variables that could potentially promote the sustained transmission of COVID-19 in their study in Mexico City in a situation designed for not wearing a mask for protection. On the other hand, López-Feldman et al. [19] found evidence of a positive relationship between air pollution by PM2.5 and the probability that an individual will die after contracting COVID-19 in their case study developed in the city of Victoria, Mexico.

According to Asadi et al. [6] and Morawaska et al. [20], in a face-to-face conversation between a pair of individuals, there is an expulsion of particles with diameters between 0.8 and 2 microns for respiration events, while, when talking, there are particles up to 7 microns dispersed by the individuals. By using facial device protection, such as face masks or respirators, it is likely to reduce the risk of disease transmission even when there is no social distance between people. Pendar and Páscoa [21] suggest a minimum of 4 m of social distance derived from their analysis of the length and width of the exhaled droplets from events of coughs and sneezes and found that the trajectories of the particles are influenced by their size, angle, velocity, and environment. Therefore, masks and their protective properties should facilitate health care and the reduction of pathogen dispersion to promote their use in situations of health contingencies where social distancing is required [22].

Based on a recent literature review, there are studies that have analyzed the efficiency of particle filtration in conventional masks and their comparison with surgical masks with N95 standards, particularly for protection against the disease generated by the SARS-CoV-2 [14]. It was found that masks made of cotton with a vacuum cleaning bag section or including a piece of wet towel (baby wipe) have a viral filtration efficiency of 99.5% [23]. Masks made with other fabrics have an efficiency of lower than 50% [24]. Dbouk and Drikakis [25] applied a new criterion to evaluate the efficiency of a face mask's performance considering the penetration dynamics of airborne droplet transmission and the leakage around the mask edges and one of their main conclusions is that wearing a commercial mask does not provide complete protection and it is necessary to maintain social distance. Thus, it is possible to improve the performance of the filter zones of a fabric mask only by incorporating layers of materials of daily use or enhancing the mask geometry and design.

On the other hand, few studies focus on an aerodynamic and comfortable design of masks. Currently, the problem around the discomfort generated by the continuous use of masks is mainly by users of the health sector, or even all those who have close contact with other people, such as waiters, taxi drivers, salesmen, among others, and otherwise those who use the masks for a prolonged and continuous time during the day. In addition, it is worth mentioning that users with respiratory problems do not use masks due to the sensation of suffocation, headache, shortness of breath, and dizziness caused by the inadequate exchange of exhalation and inhalation flows [26].

Recent studies have focused on the analysis of the performance of facial masks and have found that there are some deficiencies with respect to the geometric design, as well as in the seal with the face. Indeed, Siddhartha et al. [27] experimentally analyzed the flow through homemade fabric masks with optical techniques and their comparison with cone-type masks (KN95) for coughing and sneezing events. Among their main findings, they identified the presence of several leakage zones in all the mask models analyzed.

These areas of leakage occurred mainly in the upper area of the nose because there was no airtight seal of the mask with the face. Although the use of masks reduces the dispersion of the exhaled air cloud, their poor design promotes a feeling of discomfort in the wearer, generates fogging of the lenses when they are worn, and represents false protection for the wearer's health.

Siddhartha et al. [28] also performed an analysis of the dispersion of exhalation flows using optical techniques. They compared the performance of various types of masks and respirators with an exhalation valve, as well as a comparison with a face shield. In their work, they emphasize that, with the use of facial protection, the dispersion of exhaled air is reduced; however, this is not generated effectively when there is a dispersion of the air that travels great distances around the mask and the mask with valves. In their work, they suggested improving the design of a mask that can reduce the flow and dispersion of exhaled air in the environment.

As described in Martinez-Perez et al. [29], the existence of non-sealed areas between the mask and the face can generate health problems, such as dry eyes. It was found that most people presented symptoms of visual diseases caused by the continuous mask usage. Furthermore, people change contact lenses more frequently compared with before the pandemic and the need of wearing a mask. In this context, the mask has been accepted with more difficulty by the users because of such symptoms related to the deficient seal and design of a mask.

Other studies have used techniques such as computational fluid dynamics (CFD) in the simulation of the operation of conventional cone-type FFR masks (KN95 respirator) to verify that their use can avoid the dispersion of particles associated with the SARS-CoV-2 in closed environments. The particles exhaled when coughing can travel up to a distance of 2.6 m, and this distance can be reduced to 0.48 m and 0.73 m with the use of surgical or conventional masks according to the information reported in Khosronjejad et al. [30]. However, in studies where it is possible to reduce the dispersion of particles, the correct functioning of the mask is not guaranteed because it does not have an airtight seal or an adequate exchange of flows in the events of inhalation and exhalation to offer greater comfort to the user.

Cornejo et al. [31] made a CFD simulation considering the effect of the turbulent flow in the aerodynamic dispersion of droplets and aerosol coming from people during respiratory events. They found a significant droplets transport effect considering the action of the turbulent airflow. Particles up to 900 microns can be spread up to 5 m, and particles up to 200 microns can be dispersed at distances up to 18 m by the action of the airflow and turbulence. It is important to consider the wind velocity in the spread of droplets out of the mask to mitigate the propagation of the particles at longer distances.

Lei et al. [26] analyzed the flows through an FFR N95 mask using computational fluid dynamics (CFD) and optical techniques with an infrared camera (IRC). In particular, they studied the presence of different leaking gaps, highlighting that the area with the greatest leakage flow is found over the nose and eyes, followed by the cheeks. In addition, with the analysis of temperature variability, they detected that there is an increase in heat in the area near the mouth and lips, relating it to thermal discomfort for the user. In their research, the use of CFD is highlighted as an alternative for the study of fluids at a low cost and with results that allow improving the design of this type of mask.

The presence of gaps between the face and the mask reduces the volume of filtered air in the inhalation and exhalation events. This situation causes a greater dispersion of unfiltered air that favors the danger of infection between individuals. Peric and Peric [32] conducted an investigation using numerical simulation to evaluate the design and flow inside a mask used as protection against COVID-19. They analyzed the exhalation and inhalation flow with air flow rates of up to 3095 L/min considering gaps with different geometric shapes and in different areas of the face (on the nose, close to the eyes). They found that, for gaps with openings of 0.4–1 mm, 30–70% of the total flow comes out through the gaps and, in some cases, up to 80% for FFP-2 masks. Derived from this, the inherent need arises to make an

adjustment or modification to the designs of conventional masks to guarantee the largest volume of filtered air and thus reduce the risk of contagion between individuals.

On the other hand, with technological advances in the area of medicine and health, it is possible to design and manufacture devices that improve the behavior of masks. The use of technologies, such as 3D printing, PIM (plastic injection molding), CAM (computer-aided manufacturing), and CNC (computerized numerical control), among others, allows creating parts with high precision that previously, due to a lack of technology, was not possible. Additionally, the use of three-dimensional simulation technologies and the manufacture of prototypes allows establishing a design that can be verified and experimentally validated at a low cost [33].

Given the need to improve the performance and design of protective masks against the SARS-CoV-2, the objective of this work was to conceive an enhanced interior aerodynamic geometry of a mask maintaining the best filtering properties available to date and to compare the flow fields through a CFD analysis between the new geometric proposal and the FFR-KN95 mask assumed to be the best option for the protection of the user considering one of the main topics in the design of a comfortable, aerodynamic, and effective mask [34].

Governing Equations

A CFD analysis implies the solution through iterative and numerical methods of the fluid mechanics governing equations. In this study, the aerodynamics through the turbulence k-ε model was used to analyze the performance of the valves located at the interior of the mask. The Reynolds-averaged Navier–Stokes (RANS) equations of mass (1) and momentum ((2)–(4)) conservation in a tridimensional and cartesian scheme [35] were solved to obtain the velocity and turbulence fields in a stationary scheme and non-compressible state according to the absence of supersonic velocities into the mask.

$$\frac{\partial u}{\partial x} + \frac{\partial v}{\partial y} + \frac{\partial w}{\partial z} = 0 \tag{1}$$

$$\begin{aligned}\frac{\partial u}{\partial t} + \frac{\partial(uu)}{\partial x} + & \frac{\partial(vu)}{\partial y} + \frac{\partial(wu)}{\partial z} \\ = & -\frac{1}{\rho}\frac{\partial p}{\partial x} + \frac{\partial}{\partial x}\left[(\nu + \nu_T)\frac{\partial u}{\partial x}\right] + \frac{\partial}{\partial y}\left[(\nu + \nu_T)\frac{\partial u}{\partial y}\right] + \frac{\partial}{\partial z}\left[(\nu + \nu_T)\frac{\partial u}{\partial z}\right] + \frac{\partial}{\partial x}\left[(\nu + \nu_T)\frac{\partial u}{\partial x}\right] \\ & + \frac{\partial}{\partial y}\left[(\nu + \nu_T)\frac{\partial v}{\partial x}\right] + \frac{\partial}{\partial z}\left[(\nu + \nu_T)\frac{\partial w}{\partial x}\right]\end{aligned} \tag{2}$$

$$\begin{aligned}\frac{\partial v}{\partial t} + \frac{\partial(uv)}{\partial x} + & \frac{\partial(vv)}{\partial y} + \frac{\partial(wv)}{\partial z} \\ = & -\frac{1}{\rho}\frac{\partial p}{\partial y} + \frac{\partial}{\partial x}\left[(\nu + \nu_T)\frac{\partial v}{\partial x}\right] + \frac{\partial}{\partial y}\left[(\nu + \nu_T)\frac{\partial v}{\partial y}\right] + \frac{\partial}{\partial z}\left[(\nu + \nu_T)\frac{\partial v}{\partial z}\right] + \frac{\partial}{\partial x}\left[(\nu + \nu_T)\frac{\partial u}{\partial y}\right] \\ & + \frac{\partial}{\partial y}\left[(\nu + \nu_T)\frac{\partial v}{\partial y}\right] + \frac{\partial}{\partial z}\left[(\nu + \nu_T)\frac{\partial w}{\partial y}\right]\end{aligned} \tag{3}$$

$$\begin{aligned}\frac{\partial w}{\partial t} + \frac{\partial(uw)}{\partial x} + & \frac{\partial(vw)}{\partial y} + \frac{\partial(ww)}{\partial z} \\ = & -\frac{1}{\rho}\frac{\partial p}{\partial z} + \frac{\partial}{\partial x}\left[(\nu + \nu_T)\frac{\partial w}{\partial x}\right] + \frac{\partial}{\partial y}\left[(\nu + \nu_T)\frac{\partial w}{\partial y}\right] + \frac{\partial}{\partial z}\left[(\nu + \nu_T)\frac{\partial w}{\partial z}\right] + \frac{\partial}{\partial x}\left[(\nu + \nu_T)\frac{\partial u}{\partial z}\right] \\ & + \frac{\partial}{\partial y}\left[(\nu + \nu_T)\frac{\partial v}{\partial z}\right] + \frac{\partial}{\partial z}\left[(\nu + \nu_T)\frac{\partial w}{\partial z}\right]\end{aligned} \tag{4}$$

where u, v, and w are the velocity, ρ is the fluid density, p is the absolute pressure, ν is the kinematic viscosity of the fluid, and ν_T is the eddy viscosity.

The k-ε turbulence model was selected because it offers a good approximation of the estimation of the turbulent kinetic energy (k) and the dissipation rate (ε) in circular flows, confined fluids that have considerable Reynolds stresses in the domain. Computationally, it is one of the most efficient and reliable models [35,36].

$$\frac{\partial k}{\partial t} + \frac{\partial(uk)}{\partial x} + \frac{\partial(vk)}{\partial y} + \frac{\partial(\rho wk)}{\partial z} = \frac{\partial}{\partial x}\left[\frac{\nu_T}{\sigma_k}\frac{\partial k}{\partial x}\right] + \frac{\partial}{\partial y}\left[\frac{\nu_T}{\sigma_k}\frac{\partial k}{\partial y}\right] + \frac{\partial}{\partial z}\left[\frac{\nu_T}{\sigma_k}\frac{\partial k}{\partial z}\right] + (P - D) \tag{5}$$

$$\frac{\partial \varepsilon}{\partial t} + \frac{\partial(u\varepsilon)}{\partial x} + \frac{\partial(v\varepsilon)}{\partial y} + \frac{\partial(w\varepsilon)}{\partial z} = \frac{\partial}{\partial x}\left[\frac{\nu_T}{\sigma_\varepsilon}\frac{\partial \varepsilon}{\partial x}\right] + \frac{\partial}{\partial y}\left[\frac{\nu_T}{\sigma_\varepsilon}\frac{\partial \varepsilon}{\partial y}\right] + \frac{\partial}{\partial z}\left[\frac{\nu_T}{\sigma_\varepsilon}\frac{\partial \varepsilon}{\partial z}\right] + \frac{\varepsilon}{k}(C_{\varepsilon 1}P - C_{\varepsilon 2}D) \tag{6}$$

$$P = 2\nu_T\left[\left(\frac{\partial u}{\partial x}\right)^2 + \left(\frac{\partial v}{\partial y}\right)^2 + \left(\frac{\partial w}{\partial z}\right)^2\right] + \nu_T\left[\left(\frac{\partial u}{\partial y} + \frac{\partial v}{\partial x}\right)^2 + \left(\frac{\partial v}{\partial z} + \frac{\partial w}{\partial y}\right)^2 + \left(\frac{\partial w}{\partial x} + \frac{\partial u}{\partial z}\right)^2\right] \tag{7}$$

where:

$$D = \varepsilon = \frac{\nu_T}{\sigma_\varepsilon} \tag{8}$$

$$k = \frac{\nu_T}{\sigma_k} \tag{9}$$

$$\varepsilon = \frac{\nu_T}{\sigma_\varepsilon} \tag{10}$$

$$\nu_T = \frac{C_\mu k^2}{\varepsilon} \tag{11}$$

k is the turbulent kinetic energy; ε the dissipation rate of the kinetic energy; ν_T is the eddy viscosity; σ_k, σ_ε, $C_{\varepsilon1}$, $C_{\varepsilon2}$, and C_μ are adjustable constants according to the experimental data proposed and described in literature [36–38].

The filter medium idealized as porous media was defined to simulate the flow resistance through the filter areas. Assuming laminar flow, the pressure drop is proportional to the flow velocity and the Darcy's law (12) replaces the momentum equation.

$$\nabla p_a = -\frac{\mu_a}{\alpha}\overline{V}_a \tag{12}$$

where μ_a is the air viscosity, $1/\alpha$ is the viscous resistance coefficient (1/m), V_a is the air velocity, and p_a is the pressure. The viscous and inertial resistance coefficients are described in [38] and can be estimated with the expressions ((13) and (14)), respectively, and are used in the Ergun Equation (15).

$$\frac{1}{\alpha} = 150\frac{(1-e)^2}{\phi^2 D^2 e^3} \tag{13}$$

$$\frac{1}{\alpha^2} = 3.5(1-e)/\left(\phi D e^3\right) \tag{14}$$

$$\frac{\Delta p}{\Delta L} = \left(\frac{1}{\alpha}\mu_a V_a\right) + \left(\frac{1}{2\alpha^2}\rho V_a^2\right) \tag{15}$$

where $\frac{\Delta p}{\Delta L}$ pressure drops per length unit, μ_a is the dynamic viscosity, ρ the fluid density, e the porosity of the medium, ϕ the sphericity of the particles making the medium, and D the diameter of the particles making the medium.

For the static structural analysis, the stress–strain relationship for linear materials was used, where the stress is related to the strain according to the Equation (16).

$$[\sigma] = [D]\left\{\varepsilon^{el}\right\} \tag{16}$$

where $[\sigma]$ is the stress vector known as $S = \begin{bmatrix} \sigma_x\ \sigma_y\ \sigma_z\ \sigma_{xy}\ \sigma_{yz}\ \sigma_{xz} \end{bmatrix}^T$; $[D]$ is the elasticity or elastic stiffness matrix; $\left\{\varepsilon^{el}\right\}$ elastic strain vector. The elastic stiffness matrix depends on Young's modulus (E), Poisson's ratio (ν), and the shear modulus (G). These properties are specified according to the material used in the analysis.

2. Materials and Methods

Geometric Proposal

The geometric proposal of the mask was made based on the mathematical expectation of the anthropometric dimensions of a young adult person [39]. For this, the preliminary sizing considered the dimensions of the surgical masks (FFR) KN95 and KN99. The final dimensions of the proposed mask were adjusted based on the analyzed internal aerodynamic components that guaranteed the enhanced gas exchange of the respiration process.

To improve the performance of the mask, various geometric proposals were made by modifying each of the main components that make it up, particularly the number, size, and position of the valves. Figure 1 shows the enhanced geometry proposed in this work. The final components are made up of static valves in the form of a spiral, deflectors, and internal ducts that facilitate the flow of air to the different outlet and inlet zones, avoiding stagnation and recirculation within the mask. Figure 2 shows the details of the mask and the location of the valves that have the objective of favoring a greater mass flow of air in one direction than in another. Front static valves were designed to achieve efficient exhalation flow. The other two valves located near the face were designed to facilitate inhalation flow. The valves are attached to a plate that contains a copula that separates the exhalation flow, directing it to the lower ducts.
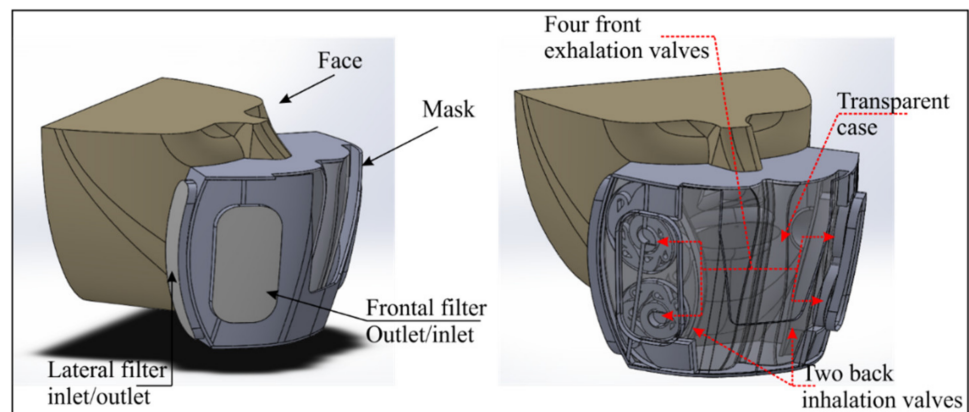

Figure 1. Geometric model of the mask and its main components.
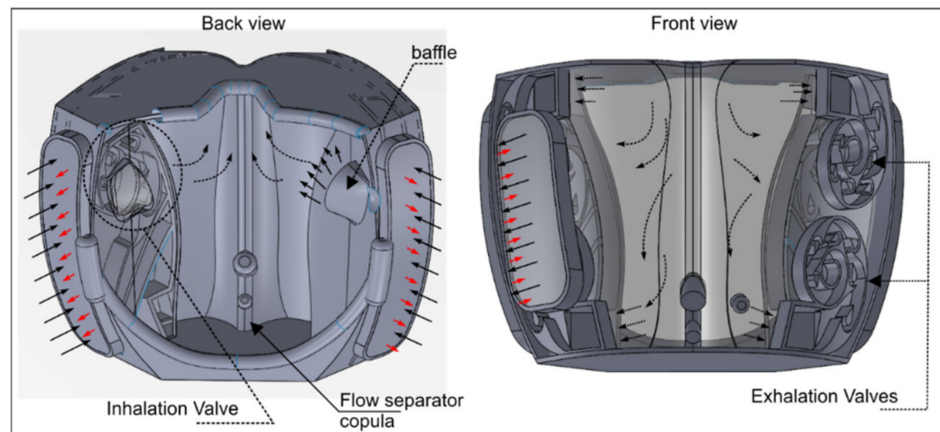

Figure 2. Interior view of the mask. The back view shows the valves and baffles for inhalation events, and the front view shows the valves for exhalation events.

The proposed geometric design for the valves was established based on the aerodynamics of a converging spiral to channel the flow towards the area of interest. At the same time, it was sought to vary its velocity according to the direction in which the air flows to promote the flow separation and directing it to the exhalation and inhalation valves. Deflectors (baffles) with aerodynamic geometry were placed inside the spirals to channel the flow in one direction, while, in the other direction, the generation of vortices and velocity fluctuations was promoted to limit the free flow of air. While inhaling, the four frontal valves operate by generating a chaotic flow, slowing the flow rate due to the turbulence generated. At the same time, the two valves near the face and whose exit are towards the lateral zones allow the entry of the flow through a gradual convergence, accelerating the flow towards the interior of the mask and directing the air towards the

nose. During the exhalation phase, the flow that comes out through the nose or mouth is directed through the four valves whose convergent geometry facilitates the exit of air through the frontal area to the outside of the mask. At that same moment, the valves near the face with exit to the lateral zones produce a turbulent flow thanks to the internal deflectors and the divergence of the spirals. Figure 3 shows the operating diagram of the spiral valves for the inhalation and exhalation events. The location and geometry of the spirals and baffles were established to have predominant inhalation flows in the lateral valves and a predominant exhalation flow in the frontal valves.
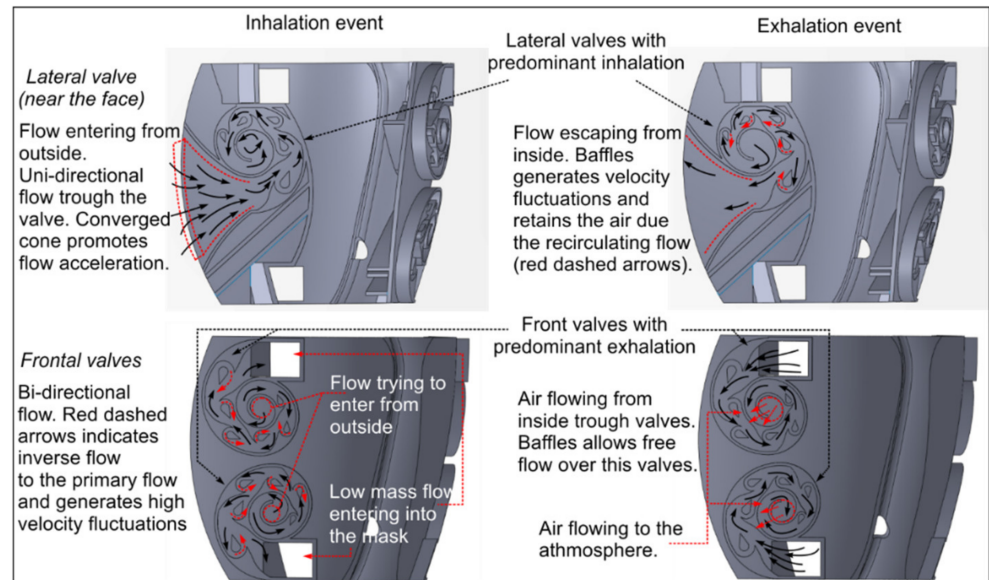

Figure 3. Description of the valves for inhalation and exhalation events.

To evaluate the performance of the proposed mask, a set of experiments and scenarios were performed that were simulated by CFD to later contrast them with the results of the base scenario without the spiral filters (porous media) and with a commercial mask FFR-KN95. Figure 4 shows the geometries of the three masks proposed and the events analyzed by CFD for the evaluation of the velocity and turbulence fields, as well as their efficiency in the inhalation and exhalation of the air volumes in each zone.
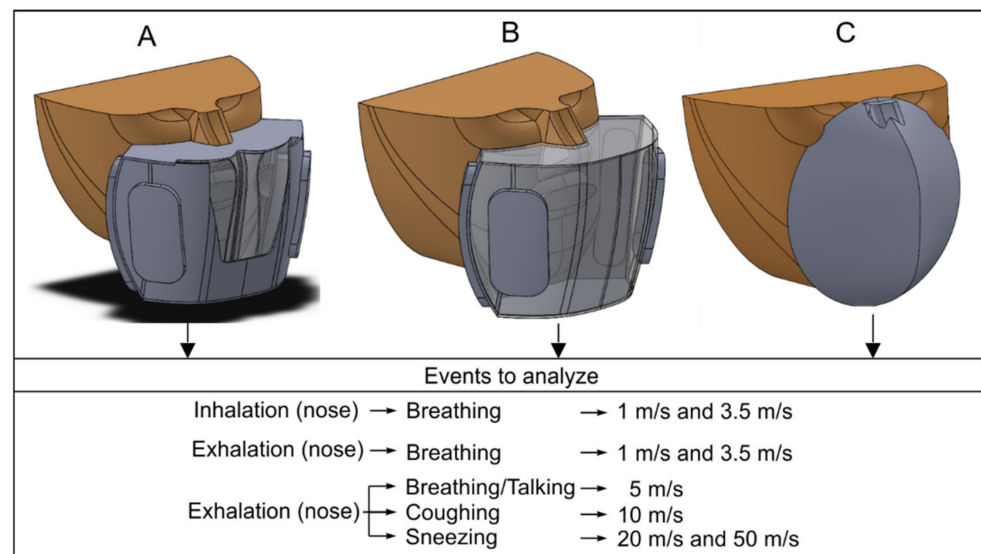

Figure 4. Comparison of the mask geometries analyzed with CFD; (**A**) mask with interior static spiral valves; (**B**) mask without interior valves, and (**C**) KN95 commercial respirator.

For the CFD analysis, ANSYS © software was used, and the procedure suggested by ANSYS [38] was followed. The first stage was obtaining the computational fluid domain (volume of air), which is the control volume confined between the inner part of the mask and the face. To extract the air domain of the mask, it was necessary to generate the geometry of the mask, and then a Boolean operation was applied to obtain the fluid of the mask interior, which was the control volume discretized into a three-dimensional mesh. This control volume was spatially discretized through an unstructured hybrid mesh with tetrahedral and hexahedral elements of different sizes to ensure the fit to the complex internal geometry of the mask. The outlet zones that correspond to the filters were meshed with an inflation tool to obtain up to ten elements in the 1 mm layer thickness of the filter zone to guarantee the convergence solution of the porous media model applied. Mesh sensitivity analyses were performed evaluating different element sizes from 10 to 2 mm maximum and 1 to 0.025 mm minimum. Monitors of the velocity, pressure, and turbulence fields at boundaries and interior of the domain were evaluated. Figure 5A shows the conceptual model of the mask with inner valves, and Figure 5B shows the inner fluid domain. Figure 5C shows the details of the control volume mesh. This same procedure was performed for each of the masks analyzed.
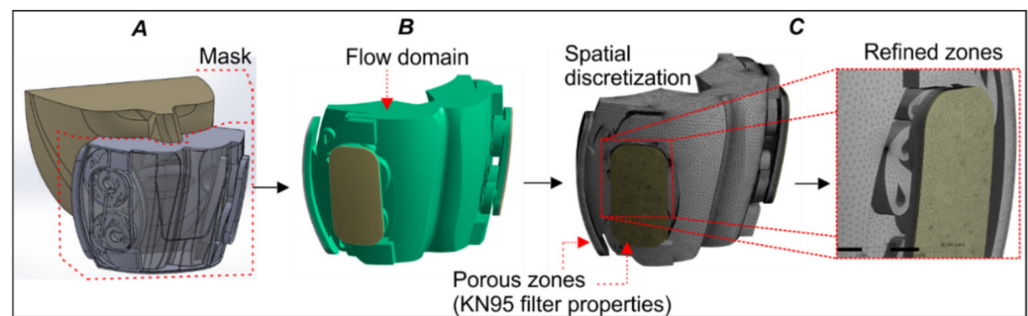

Figure 5. Control volume and spatial discretization of the air domain into the mask. (**A**) Mask geometry; (**B**) computational flow domain considering porous zones; and (**C**) spatial discretization of control volume.

The boundary conditions and the velocity values used for the analysis of the masks are shown in Table 1. For the FFR-KN95 mask, the operating scenario was constructed considering the case with a hermetic perimeter seal with a gap of 1.3 cm^2 in the upper area of the nose. For all simulation cases, the values of the mouth opening area of 4.25 cm^2 were conserved and for each nostril of 0.78 cm^2, as described in literature [23,26,32]. The area of the KN95 respirator was established at 114 cm^2 according to the actual dimensions of the product. For the case of the mask proposed in this research, an area of 17.8 cm^2 was established for each front filter, while, for each lateral filter, there was an area of 14.6 cm^2, giving a total filtering area of 64.8 cm^2, which was 54% of the area of a KN95 respirator. This guarantees the entry and exit of the flow for all respiratory events. The air flow for each case was established according to what was described in literature [10,26], where there are respiration velocities of 1 and 3.5 m/s associated with flows of 9.5 and 33 L/min, respectively, and an additional event of speaking with an air velocity of 5 m/s on exhalation [9]. For violent events of coughing and sneezing, exhalation velocities with magnitudes of 10, 20, and 50 m/s were considered. The air velocities and flows were established according to what was described in literature [8–10,13,22,40–42]. According to the geometry of each mask, the inlet velocity and outlet pressures were applied in the areas where the filters were located. Figure 6 illustrates the areas in the control volumes where the mentioned boundary conditions were applied.

Table 1. Boundary conditions and main parameters considered in the mask simulation.

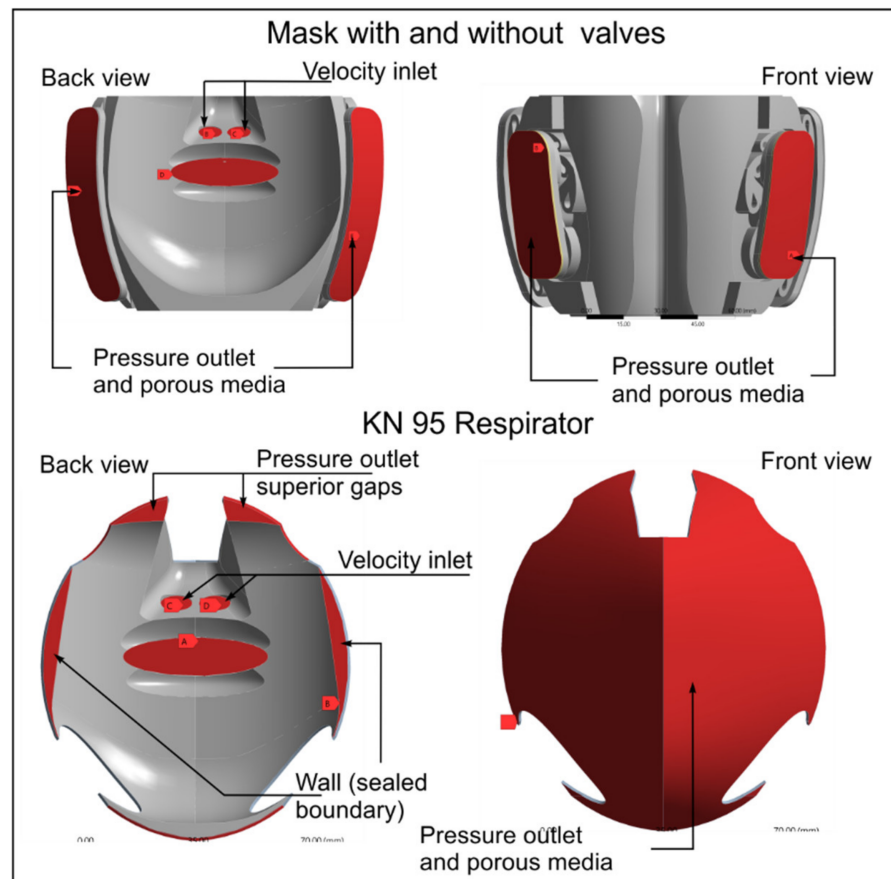| Boundary Conditions					
Mask	Boundary	Element	Parameter	Value	Notes
Mask with valves and Mask without valves	Velocity Inlet.	Cross-sectional area of nose orifices.	Flow velocity-inlet on each orifice	1 (m/s) for exhalation and −1 m/s for inhalation	Speed established considering inhalation and exhalation of a young and healthy person.
		Cross-sectional area of nose orifices.	Flow velocity-inlet on each orifice	3.5 (m/s) for exhalation and −3.5 m/s for inhalation	
		Cross-sectional area of mouth according to	Flow velocity-inlet	5 (m/s) exhalation	Breathing/talking case
				10 (m/s) exhalation	Coughing case
				20 and 50 m/s exhalation	Sneezing cases
	Outlet	Lateral and frontal filters area	Gauge pressure	0 atm	Atmospheric pressure at sea level.
KN95 respirator	Outlet	Superior gaps above the nose according to [27,28]	Gauge pressure	0 atm	Atmospheric pressure at sea level.

Figure 6. Boundary zones for each mask and respirator KN95.

According to the information on inhalation and exhalation velocities reported in the literature, the boundary and initial conditions are established considering the onset of each event. The velocity input used in the boundary condition is assumed to be the terminal velocity of the event and comes from the nose or mouth. For the initial condition of the analysis, it is assumed that the air entering the mask begins to move from its rest for each event.

An important stage in the CFD simulation was the refinement of the mesh to achieve satisfactory convergence. A mesh with tetrahedral elements with a minimum size of 0.025 mm and a maximum of 2 mm was used. Table 2 shows the mesh quality and number of elements for each case of the mask and respirator analyzed. The methods and factors used in the numerical models available for the analysis are also shown, highlighting the use of the κ-ε turbulence model. The simulation was proposed in a quasi-stationary scheme because the interest in this research was to know the final state of the flow and verify the performance of each mask within the first 1.5–2 s, which is the maximum time that an event of exhalation or inhalation occurred, as described in literature [41,43].

Table 2. Parameters and values for mesh and setup for the simulation.

Mesh Properties of the Model				
Orthogonal Quality Index	**Value**	**Number of Elements for Each Quality**		
		Mask with Valves	**Mask without Valves**	**KN95 Mask**
Minimum (acceptable mesh)	0.1–0.4	~50,000	~15,000	~40,000
Medium (good mesh)	0.5–0.9	4.8 million	4.35 million	7.33 million
Maximum (excellent mesh)	0.99			
Methods and factors used in the simulation				
Term	**Relaxation factor**	**Interpolation method**	**Characteristics**	
Gradient	-	Green-Gauss Cell Based	Minimize cell variation	
Pressure	0.3	PRESTO!	Rotational flow and curved geometries.	
Momentum	0.7	Second Order Upwind	High accuracy in the residuals.	
Turbulent Kinect energy	0.8	QUICK	For tetrahedral mesh and rotational flows.	
Turbulent dissipation rate	0.8	QUICK		

The behavior of the flow was assumed to be in a steady state (not transient); continuity, momentum, and κ-ε turbulence equations where activated. Air properties at 15 °C was established. 2500 iterations were made by the software to achieve the final solution.

It is important to note that the analysis of the flow considering the filters at the entrance and exit boundaries of the masks and the KN95 respirator is a very complex phenomenon involving several variables that, in practice, are difficult to measure, such as the structure of the filter filaments, the vacuum that exists within the material, the internal roughness that causes friction, and energy loss. The filter medium contains fibers arranged randomly, which causes flow resistance, and the laminar flow velocity is proportional to the pressure drop through the porous medium. Thus, in this work, the Ergun equations and Darcy's law were considered, which modified the Navier–Stokes equations for the modeling of porous media, establishing the parameters and values shown in Table 3 as described in [23,26,34,39,44,45]. It is worth mentioning that the values adopted in the simulations may vary slightly when compared with experimental cases. The main parameters in the analysis of the porous media are the viscous and inertial resistance, and those were established considering the pressure drop of 26.5 Pascal and 155 Pascal for the breathing (33 lpm) and talking (126.8 lpm) cases, respectively, in the KN95 respirator filter reported in [26,46]. For the Darcy's equation, it was important to consider the particle properties, such as diameter of 0.3 microns and porosity of 0.85, suggested by [23,47]. The outlets of the mask were selected as the zones for the porous media, which are 1 mm thickness, as shown previously in Figure 6. The strategy of this work was to maintain the same parameters in the filtering zones for all cases of the masks and the respirator to contrast its operation under the same conditions of porous medium and to offer a more realistic approximation of the mask performance.

Table 3. Parameters and values adopted in the modeling of the porous medium considering the Ergun equations and Darcy's law.

Parameter	Adopted Value	Source
Air density, ρ	1.225 kg/m^3	-
Air dynamic viscosity, μ	1.79×10^{-5} kg/(m s)	-
Porosity, e.	0.85	[23,26]
Sphericity of particles making the medium, ϕ.	0.75	Mean value between 0.5 (deformed) and 1 (spherical)
Diameter of particles making the medium, D.	0.3 μm	[23]
Thickness of the porous zone	1 mm	[30]
Viscous resistance, $1/\alpha$.	634,293,552,812 m^{-2}	Calculated with [38] simplified Ergun equation
Inertial resistance, $1/\alpha^2$.	3,917,695 m^{-1}	Calculated with [38] simplified Ergun equation

The parameters used for the analysis of porous media can change according to different authors and the characteristics of each product (filters) on the market. However, in this research, certain values suggested by the literature were adopted with the objective of observing the change in the flow fields due to the presence of filters at the boundaries and making a comparison with the case where the filters are not available.

The geometric design and aerodynamic performance of the mask, as well as the valves, are guaranteed if there is a tight seal with the face, a situation not commonly encountered with most commercial masks or respirators. In the present work, a basic static structural analysis in a static scheme of the mask with the seal on the face was carried out. This was done to evaluate the most suitable position of the mask holding brackets to ensure there is sufficient sealing pressure on the face to avoid areas of leakage. For this, the pressure and stress field on the seal was analyzed to verify the existence of deformations around the perimeter of the seal in contact with the face.

It was assumed that the internal pressure generated by the fluid should be equal to or less than the pressure on the seal and the face due to the mask holding brackets but in the opposite direction, maintaining a uniform pressure and deformation distribution on the seal against the face and mainly in the upper area of the nose. For the structural analysis approach, ANSYS Static-Structural software was used. Regarding the mechanical properties of the components, different material was assigned: plastic (PET) for the mask, silicone for the seal, and polyethylene to idealize the flexibility of the face. For the boundary conditions, the forces were applied on each surface of the proposed holding brackets, and the back of the face was idealized as a fixed support condition where there is no displacement or deformation in any of the directions. The conceptualization of the materials and boundary conditions for the structural analysis are shown in the Figure 7.
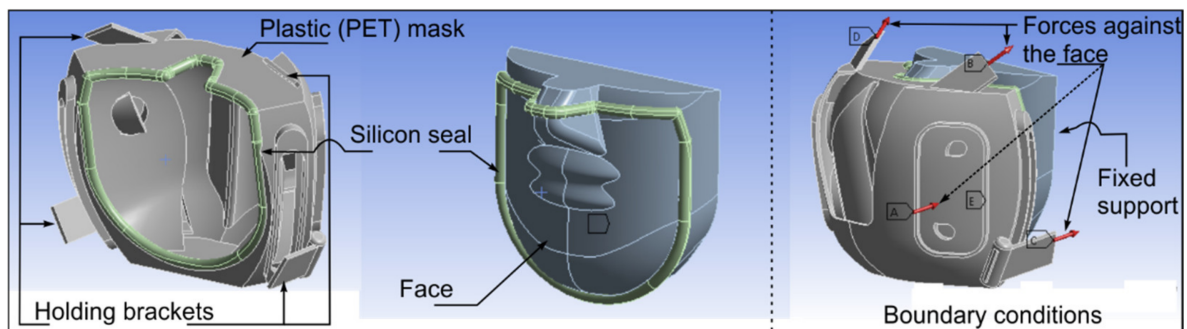
Figure 7. Conceptualization of the mask, seal, and face for the static structural analysis.

3. Results and Discussion

The results of the CFD analysis are shown graphically, in particular the velocity and turbulence fields of the mask prototype with internal valves without considering filtering media. To appreciate the operation of the inner valves, the results of the flow fields for inhalation and exhalation events in the nose at a velocity of 3.5 m/s are shown. Figure 8 shows the velocity fields for the inhalation and exhalation events in a lateral plane located in the middle of the inner valves. In this figure, it can be observed that the air flows with greater velocity in the frontal valves whose objective is the air outlet (Figure 8a), and this velocity is much lower in the inhalation event for the same valve zone (Figure 8c). With respect to the behavior of the valve system for the inhalation event, there is a higher velocity in the lateral valves whose objective is to favor the entry of air (Figure 8d), and this velocity is significantly reduced in the same area when the event of exhalation (Figure 8b) restricts free flow in this area.
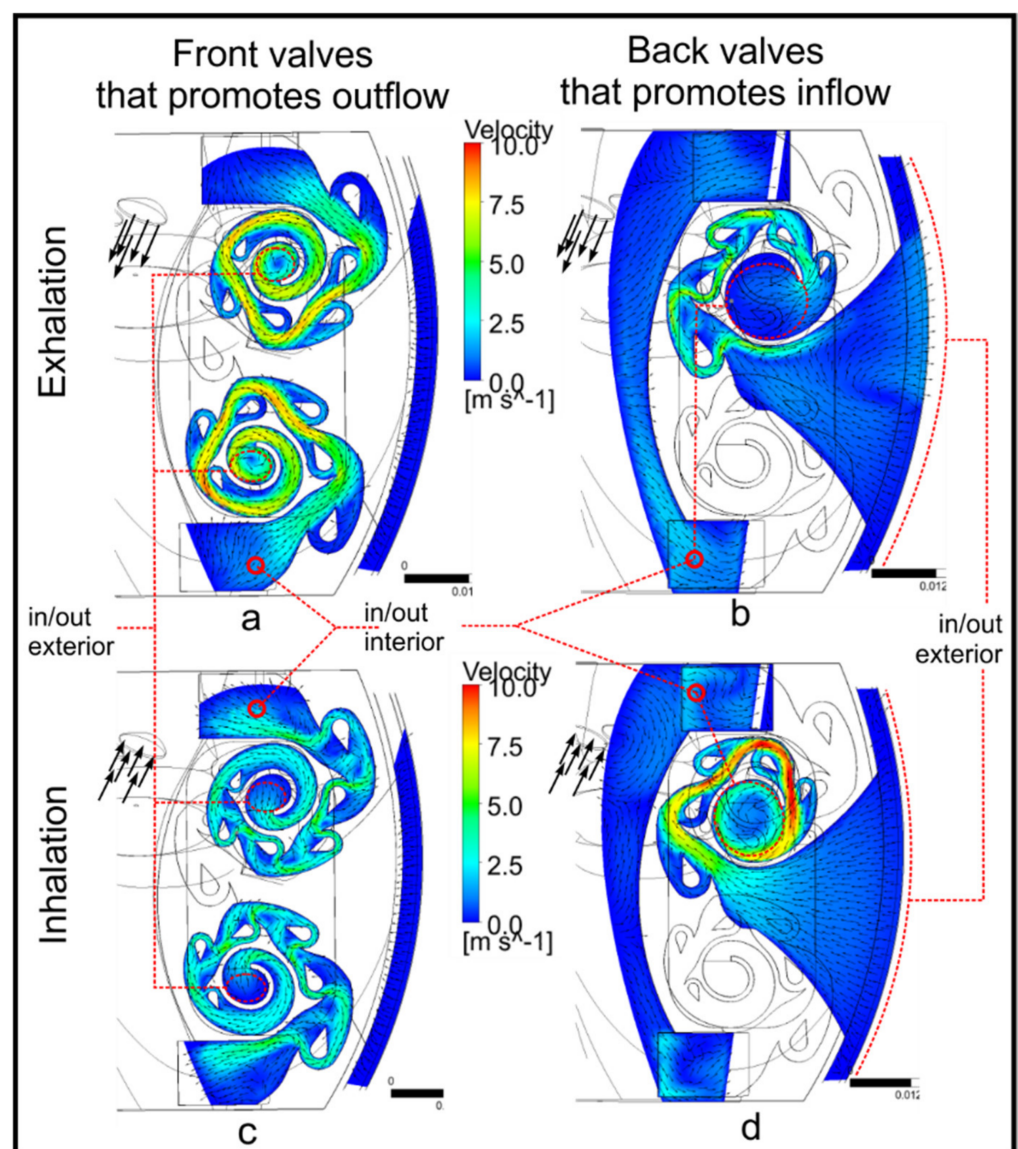

Figure 8. Contours of velocity flow into the mask. (**a**) Exhalation through valves that promote outflow; (**b**) exhalation through valves that promote inflow; (**c**) inhalation through valves that promote outflow; and (**d**) inhalation through valves that promote inflow.

The effect that occurs inside the valves to promote flow in one direction and restrict it in the other is attributed to the innovative geometric design of the ducts and baffles that generate velocity fluctuations associated with turbulence. Figure 9 shows the turbulence fields in each valve in the inhalation and exhalation events for a velocity of 3.5 m/s in the mask without considering filtering media. It is observed that the performance found of the orientation and shape of the baffles effectively promotes the shock of flows and velocity fluctuation in the valves shown in Figure 9b,c for the exhalation and inhalation events, respectively. Figure 9a,d shows that there is turbulence in the range of 0.9–2.6 m^2/s^2; however, the air flows uniformly, as indicated by the vectors, and there is less turbulence at the inlets and outlets of the flow.
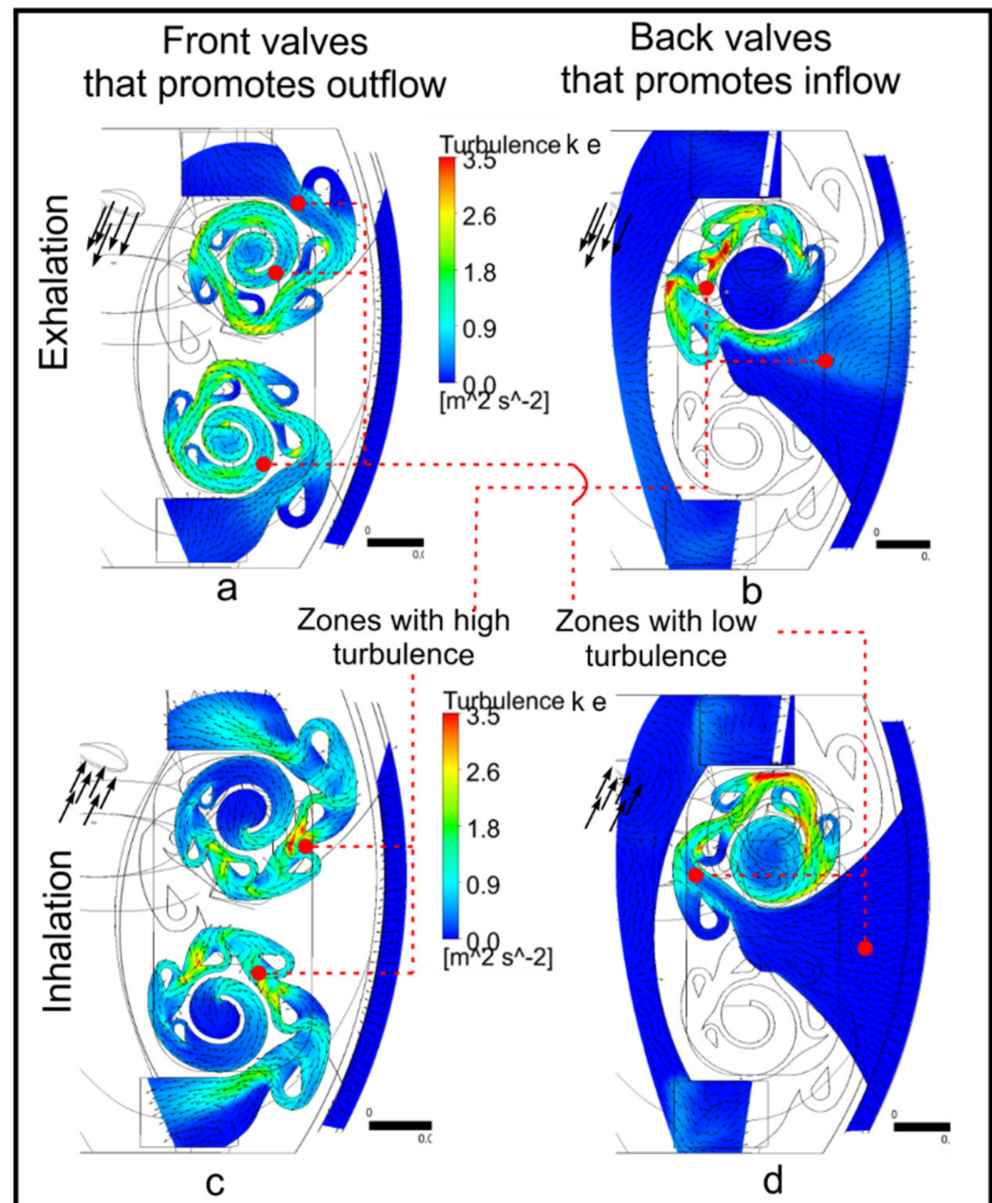

Figure 9. Contours of turbulence Kinect energy into the valves. (**a**,**d**) show zones with low turbulence in the valves for exhalation and inhalation events, respectively. (**b**,**c**) show zones with high turbulence due to baffles for the exhalation and inhalation events, respectively.

The aerodynamic analysis of the proposed mask allowed us to know the mass flow that enters and leaves each of the valves for the inhalation and exhalation events. According to the inhalation and exhalation velocities described in the literature, it is possible to know the mass flow that a person inhales and exhales through the nose and mouth [26]. Thanks to the CFD analysis, it was possible to compare the inhalation and exhalation flows in the different inlets and outlets of the mask proposed in this work. The priority that was established in the geometric design of the mask was to achieve the rapid and effective exit of the air through the front of the mask in the event of exhalation, avoiding the stagnation of the flow within the mask. On the other hand, the proposed geometric design allows the prioritization of air intake from the lateral area of the mask, and the flow is directed towards the nose for early inhalation, thus avoiding breathing again the air that had previously been exhaled from the front. This ensures the flow exchange, a situation that is not found with any of the conventional masks.

Figure 10 shows an iso-volume of the air and its velocity inside the mask and valves for the inhalation and exhalation events for a velocity of 3.5 m/s. Figure 10a,b shows that the air that comes out through the nose in the exhalation event impacts the mask and is directed towards the frontal and lateral valves, preventing its recirculation within the mask. In Figure 10c,d, the air from the lateral inlets is directed directly to the nose and mouth, ensuring that the greatest amount of air volume is inhaled during the duration of the inhalation event, which is approximately 1.5 s [26,41].
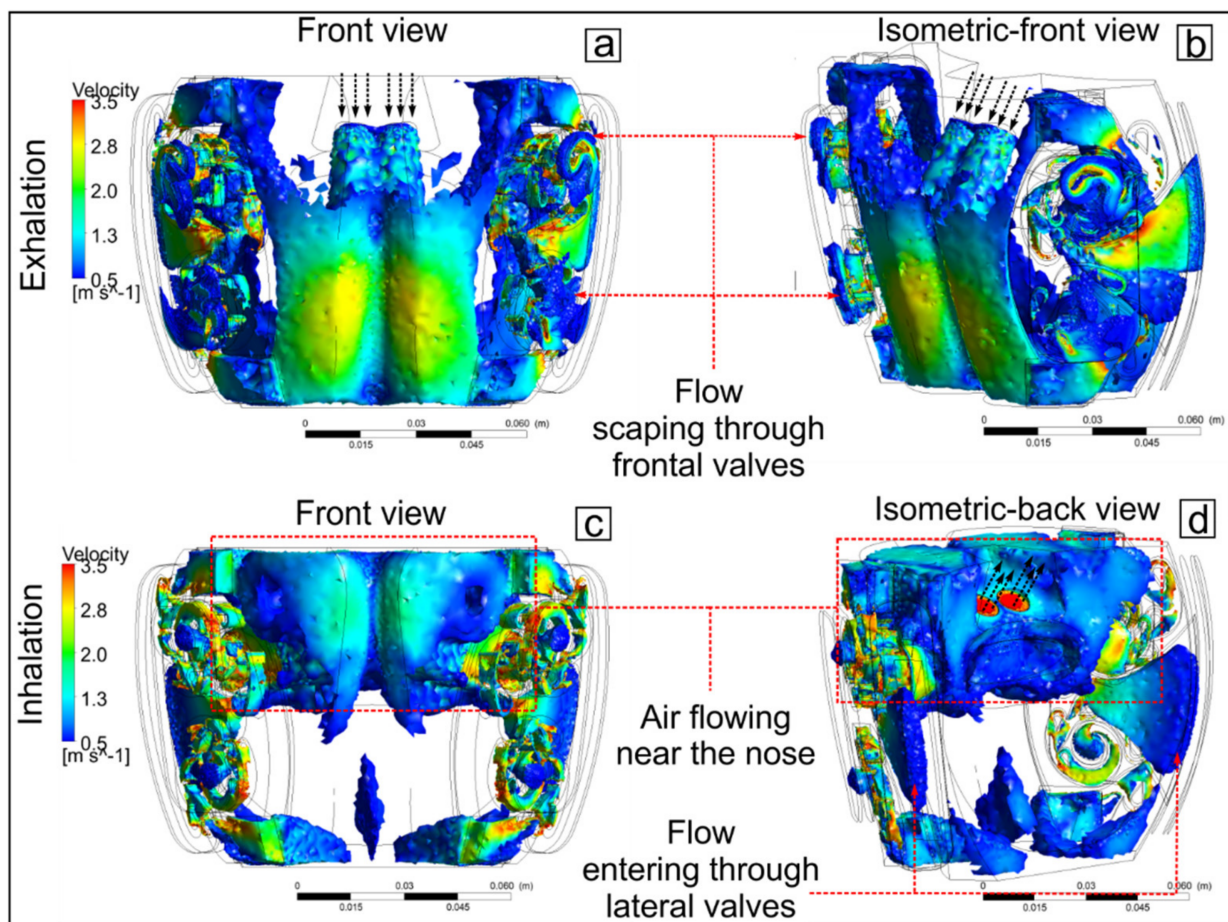

Figure 10. Iso-volume of air velocity into the mask. (**a**,**b**) exhalation event; (**c**,**d**) inhalation event.

The results obtained prove that the geometry of the valves and the mask allow an effective bidirectionality of the flow in the inhalation and exhalation events. However, to perform the functional contrast with respect to a commercial mask type KN95, it was necessary to include in the boundaries the conditions of a porous medium representing the resistance to the free flow of air through a filter with KN95 characteristics. The inclusion of the filter in the borders of the mask presented in this work decreased its efficiency with respect to the scenarios presented without filters. However, the flow exchange is still evident, as is the efficiency of the air flow towards the inlets and outlets. Likewise, it was considered important to make the comparison with the commercial mask model to demonstrate that the interior valves allow the entry and exit of air more efficiently than in those masks that do not have an interior aerodynamic design. For this, the flow fields were also compared with the geometry of the mask proposed in this work without valves and interior baffles, with the purpose of verifying that the valves effectively direct the air towards the inlet and outlet zones.

Table 4 shows the air flows and the corresponding percentage in each zone for the case of the mask with valves for different operating scenarios. For the most frequent operating scenarios, such as breathing, 62% of the air was inhaled through the lateral valves, and 38% was inhaled through the front valves. These percentages change significantly for the exhalation event, where 77% of the air leaves through the frontal valves, while 26% leaves through the lateral valves for a velocity of 3.5 m/s in the nose. For the case of respiration associated with a velocity of 1 m/s, the percentages of the air volumes change for the inhalation and exhalation events compared to the case of respiration of 3.5 m/s. However, the operation of the valves maintains a greater volume of air exhaled through the frontal area and a greater volume inhaled through the lateral areas. In addition, for the cases of talking, coughing, and sneezing, 77% of the air comes out of the frontal valves. This situation allows that, at the time of inhalation, there is an entry of clean air that enters through the side valves, avoiding the entry of air that was previously exhaled through the frontal area. This exchange of volumes in each zone and for each event was achieved thanks to the innovative geometry designed inside the spiral valves with convergent channels, thus improving the behavior of the mask proposed in this work.

Table 4. Air flow and percentages per zone and event for masks with valves and without filters at boundaries.

	Breathing at 1 m/s (Nose)		Breathing at 3.5 m/s (Nose)		Talking at 5 m/s (Mouth)	Coughing at 10 m/s (Mouth)	Sneezing at 20 m/s (Mouth)	Sneezing at 50 m/s (Mouth)
Zone/event	Inhal.	Exhal.	Inhal.	Exhal.	Exhal	Exhal	Exhal	Exhal
Lateral inlet/outlet	5.2 lpm (55%)	3.5 lpm (38%)	20.5 lpm (62%)	8.6 lpm (26%)	29.1 lpm (23%)	59.5 lpm (23%)	117 lpm (23%)	291 lpm (23%)
Frontal outlet/inlet	4.3 lpm (45%)	5.8 lpm (62%)	12.5 lpm (38%)	24.4 lpm (74%)	97.7 lpm (77%)	194.5 lpm (77%)	390 lpm (77%)	971 lpm (77%)
Total	9.5 lpm	9.3 lpm	33 lpm	33 lpm	126.8 lpm	254 lpm	507 lpm	1262 lpm

Table 5 shows the values of the air flows and the corresponding percentage in each zone for the cases of masks with valves, without valves, and the KN95 model considering filters in all cases and an entry velocity through the nose of 3.5 m/s. It is observed that the mask with valves presents a greater volume of exhalation flow in the frontal zone with 60% of the total flow. For the inhalation event, it is observed that the flow is divided into equal parts for each zone, where 50% of the total flow enters through the frontal zone while the other 50% enters through the lateral zone. With these values of air volume, it is also observed that there is a change in the behavior of the mask with valves when considering the filtering medium at the boundaries. However, this scenario offers an ideal approximation to the real behavior of masks with filter media.

Table 5. Air flow through nose: percentages per zone and event for each mask considering filter at boundaries.

Zone	Mask with Valves		Mask without Valves		KN95 Mask	
	Inhalation	Exhalation	Inhalation	Exhalation	Inhalation	Exhalation
Lateral inlet/outlet	16.2 lpm (49%)	13.3 lpm (40%)	14.8 lpm (45%)	14.9 lpm (45%)	-	-
Frontal outlet/inlet	16.8 lpm (51%)	19.7 lpm (60%)	18.0 lpm (55%)	18.1 lpm (55%)	-	-
Superior gap	-	-	-	-	31.7 lpm (96%)	34.4 lpm (95%)
Frontal through filter	-	-	-	-	1.3 lpm (4%)	1.6 lpm (5%)

For the case of the mask without valves where there are only filters at the borders, there is an inflow and outflow of the frontal zone of 55% and the lateral zones of 45%. This is achieved by idealizing a hermetic seal of the mask with the face but without internal aerodynamic movement. This case of a mask guarantees the entry and exit of air, but, with recirculation inside, a situation very similar to that of a KN95 mask. For the case of a KN95 mask, only 4–5% of the flow is in and out of the filter from which the mask is made. This causes the greatest amount of flow to enter and exit through the gaps between the face and the seal of the mask. Ninety-five percent of the air enters and exits through different areas, such as the upper part of the nose, because it does not have an airtight seal with the face, a situation that occurs with the majority of users of this type of mask [26–28,30,32].

The results shown above were obtained through CFD analysis, and, in practice, these results may vary slightly because the analysis of the porous medium applied in the simulation is numerical and simplified. However, it is a good alternative to complement the aerodynamic analysis of the mask with valves since the comparison of the flow fields with the mask without valves and the KN95 mask was performed considering the same filter conditions at the borders in all cases. Figure 11 shows the flow velocity streams for the mask with valves and baffles, the mask without valves, and the KN95 respirator considering the exhalation flow through the nose of 3.5 m/s. In Figure 11a,b, it can be observed that the air flow path flows towards the front and side valves. In addition, considering that the maximum duration of an exhalation event is 1.5 s, it is observed that, at that instant of time, the flow is already close to the outlets, guaranteeing its expulsion outside the mask. On the other hand, in Figure 11d, it is observed that there is a recirculation of the flow inside the mask by not having the valves and the baffles to direct the flow towards the outlets. Consequently, the air recirculates for approximately 2 s, a time that exceeds the maximum value of an exhalation event. This causes the air that cannot escape to the outside of the mask to be re-inhaled by the user. Finally, Figure 11e,f shows the flow velocity and exhalation timelines for the KN95 respirator, considering the frontal area as the filter and a gap over the nose. It is observed that the air leaves through the upper gap in a very short time (<0.5 s) since the geometry of the mask and the characteristics of the porous medium prevent it from leaving through the frontal area. In addition, it is observed that there is a recirculation of air in the area near the mouth, causing a sensation of suffocation for the user, as well as a headache from inhaling CO_2 when the mask is used for long periods.

The results obtained from the analysis of the mask without valves and the KN95 mask show that the flow has a longer time and recirculation path within the mask before exiting. In addition, the filters (porous medium) operate as a barrier, preventing the flow through them efficiently. By using the valves and deflectors inside the mask proposed in this work, it is guaranteed that there is no recirculation of the flow near the mouth or nose. In the case of the mask with valves, the presence of the filters in the borders allows the flow out more efficiently since the valves accelerate the air flow, so the resistance to flow caused by the filters is overcome.
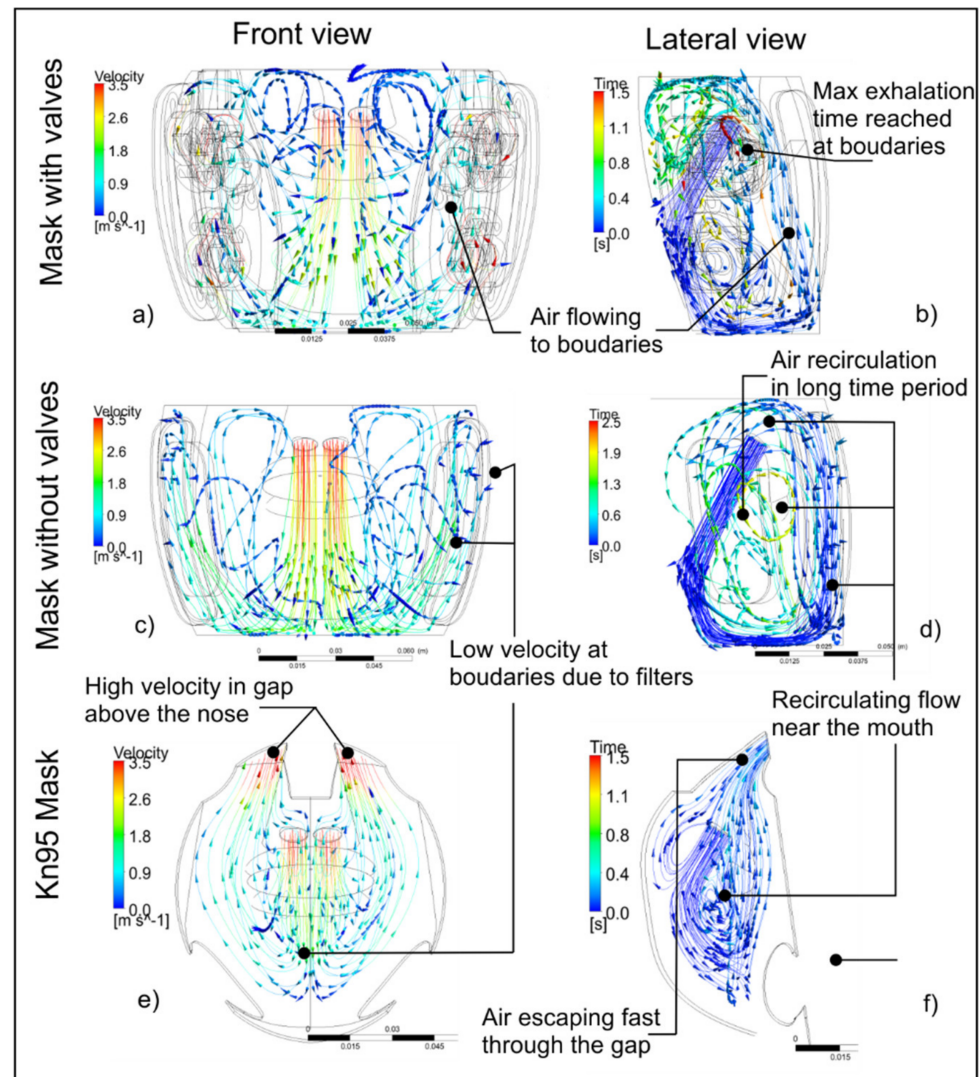
Figure 11. Streamlines of velocity and time for each mask and exhalation event at 3.5 m/s through the nose. (**a**,**b**) Case with static valves; (**c**,**d**) case without static valves; (**e**,**f**) KN95 mask case.

To verify the behavior of the outflow air in each mask, Figure 12 shows the velocity contours at the boundaries considering the exhalation event in the nose of 3.5 m/s and maintaining the filter conditions (porous medium) in all the scenarios. For the mask with valves shown in Figure 12a, the exit velocity in the frontal zone is approximately 9.5 cm/s, while the air velocity in the lateral zone is maintained at 7.5 cm/s. For the case of the mask without valves shown in Figure 12b, the flow velocity in the frontal zone is approximately 8.5 cm/s, while, in the lateral outlet, it varies between 7.5 and 9 cm/s. For the case of the KN95 mask, there is a velocity <0.5 cm/s in the frontal area (Figure 12c). This velocity occurs because the amount of air that comes out through this area is barely 5% of the total exhaled flow. The highest airflow velocity occurs in the gaps, a situation that prevents the exhaled air from passing through a filter before its release into the atmosphere.

According to the previous results, it is guaranteed that the geometric design of the valves and baffles inside the mask is effective and efficient. The results and their comparisons with the other masks showed that there is a total exchange of air within the maximum period of the inhalation and exhalation events. The enhanced geometry of the valves and baffles promotes a greater outflow in the frontal part in the exhalation, while, in the inhalation, a greater amount of air is sucked through the lateral zones. In addition, the outlet velocities in the filters do not exceed 10 cm/s. With the design and location of the valves and filters at the boundaries, a low air outlet velocity is generated to avoid

dispersion in the environment and thus reduce social distance and the danger of contagion mainly in crowded public places, such as land and air transport, schools, and offices.

It is assumed that the aerodynamic results mentioned above are valid with the existence of the seal between the mask and the face, which was an important hypothesis in this work. Therefore, as part of the structural analysis, the total internal pressure was used from the sum of the differential pressures within the fluid domain after the aerodynamic analysis. Figure 13a shows the pressure field on the inner surface of the mask. The magnitude of the force on each mask holding bracket is proportional and calculated from the internal aerodynamic pressure uniformly applied over the cross-sectional area of the seal against the face. For the exhalation event with a velocity of 3.5 m/s, the total pressure resulting from the aerodynamic analysis inside the mask is 1131 Pa and up to 1164 Pa in the surface. The perimeter area of the seal in contact with the face was proposed as 0.0015 m^2, and the total force was approximately 1.7 N. The force corresponding to each holding bracket is 0.42 N. Figure 13b,c shows the maximum stresses on the face and seal. It is observed that, in both cases, there are minimum values between 80–170 Pa and maximum values of 1600–2300 Pa. With the presence of these values, it is established that the position of the proposed holding supports in the mask allows the sufficient deformation on the seal and face that can be associated with the tightness between them, avoiding areas of vacuum or air leakage from inside the mask.
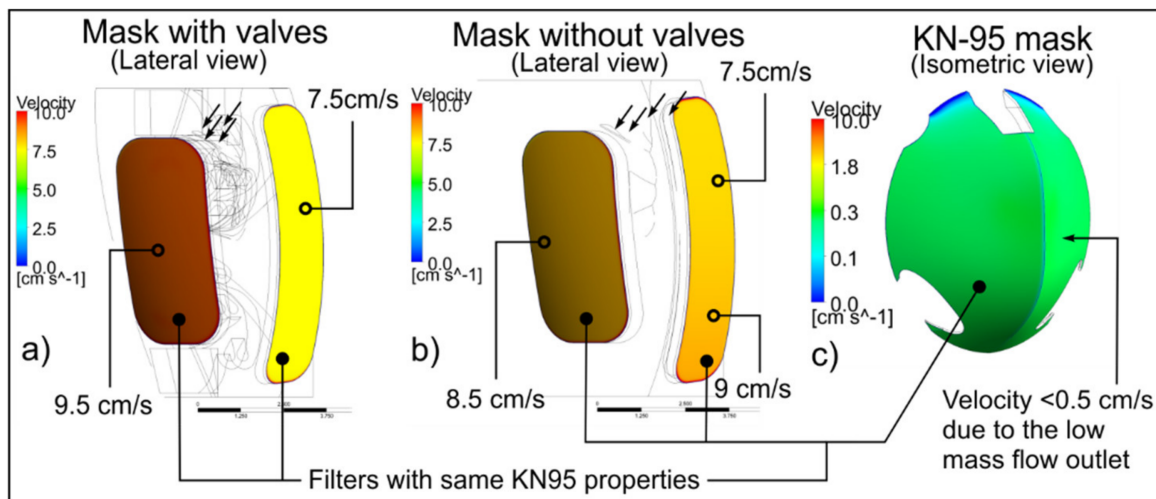

Figure 12. Contours of velocity at boundaries for each mask considering the same porous media properties. Exhalation event through nose at 3.5 m/s. (**a**) case with static valves; (**b**) case without static valves; (**c**) KN95 mask case.
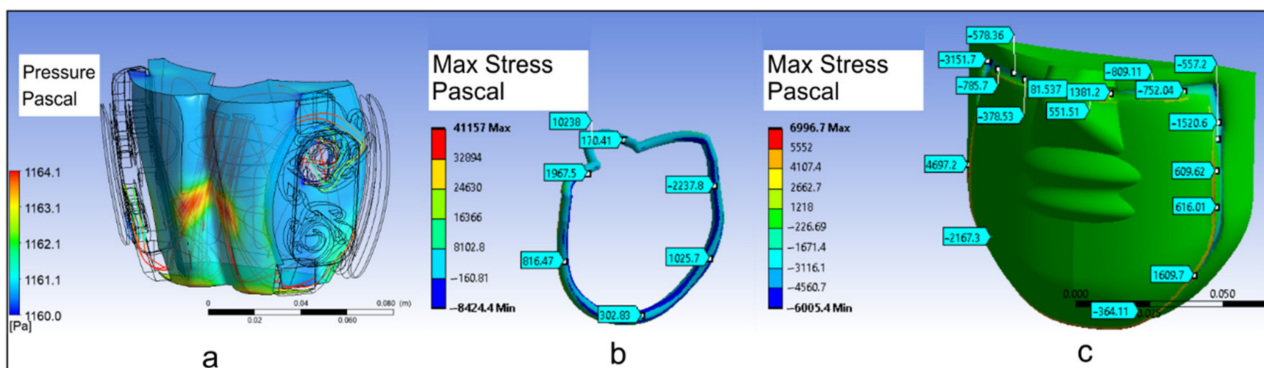

Figure 13. Contours of pressure and stress derived from the structural analysis. (**a**) Pressure contour from aerodynamic analysis; (**b**) stress over the mask seal; (**c**) stress over the contact area of the seal over the face.

By maintaining efficient aerodynamics inside the mask, the discomfort towards the user is reduced, promoting its prolonged use in daily activities. This situation will allow the user to use the mask to avoid the spread of viral and bacterial diseases in closed and public spaces. In addition, due to the COVID-19 pandemic, the World Health Organization (WHO) [1] constantly suggests the use of masks even in healthy individuals and mainly in places where it is not possible to maintain social distancing to avoid the spread of diseases among individuals. Although there is a rejection by society towards the use of masks due to the discomfort they generate, with the proposal made in this research, it is possible to offer an alternative mask with qualities of efficiency in air exchange, comfort, and reusability with a scope for civil and medical use. Thus, government health agencies in various countries can establish a mandatory use of the mask in social, economic, and service activities where there are face-to-face interactions between individuals and, at the same time, promote an acceptance of its use in society [48].

4. Conclusions

The proposal of a mask with enhanced interior aerodynamic geometry allows establishing a solution to the deficiencies of conventional masks that are usually uncomfortable and do not guarantee adequate protection for the user. The KN95 commercial masks lack a geometric design that allows adequate air exchange. In general, there is no airtight seal with the face, causing the entry and exit of air through gaps in the lateral part and mainly in the upper part of the nose. The implementation of static valves and baffles inside the mask proposed in this work allows directing the flow of inhalation and exhalation towards the inlets and outlets, avoiding recirculation at the interior. By guaranteeing a total exchange of flow, the re-inhalation of air that has been previously exhaled is reduced, offering greater comfort and convenience to the user.

The CFD analysis of the proposed mask allowed us to visualize and quantify the movement of air inside in a three-dimensional way and at a low cost. In fact, with the numerical analysis and simulation, it was possible to observe the change in the flow fields and percentages of air entry and exit in the inhalation and exhalation events. With this, it is verified that the proposed valves and baffles work correctly in two directions, allowing greater air flow in one direction and restricting it in the opposite direction. In addition, based on the various operating scenarios (breathing, talking, coughing, and sneezing), the expulsion of the greatest amount of air through the frontal zone and a greater amount of air entry through the lateral zones is guaranteed for all cases.

The analysis performed considering the filter (porous medium) at the boundaries of the masks facilitated a comparison of the flow fields, allowing the entry and exit of air even when there is the condition of flow restriction. In addition, having filters with KN95 characteristics at the borders guarantees the approval by competent health authorities for their civil and medical use because the same filtering materials of conventional masks are used. It is important to emphasize that, based on the performance comparison of the masks with the same characteristics of the filter, a better aerodynamic behavior was obtained in the mask proposed. Particularly compared to the traditional model, since the recirculation of air to the interior was avoided, it favored the efficient exit of air across the boundaries. Moreover, with the static structural analysis, it was possible to evaluate the pressure and tension between the seal and the face to guarantee an adequate support of the mask and avoid leaks around the perimeter of the seal.

Finally, the design of the internal and external components of the mask proposed in this work are intended to be manufactured at a low production cost, even with recycled PET material, and be washable and reusable, which constitutes a socially, economically, and environmentally sustainable proposal.

5. Patents

Patent under revision MX/a/2021/001476. It can be monitored at https://siga.impi.gob.mx/newSIGA/content/common/principal.jsf (accessed on 25 September 2021).

References

1. World Health Organization. Coronavirus Disease (COVID-19). Available online: https://covid19.who.int/ (accessed on 25 May 2021).
2. James, J. COVID-19: Reflections. *Disaster Med. Public Health Prep.* **2020**, *14*, E8–E11. [CrossRef]
3. Sousa, G.; Garces, T.; Cestari, V.; Florêncio, R.; Moreira, T.; Pereira, M. Mortality and survival of COVID-19. *Epidemiol. Infect.* **2020**, *148*, E123. [CrossRef] [PubMed]
4. Ibarra-Nava, I.; Cardenas-de la Garza, J.; Ruiz-Lozano, R.; Salazar-Montalvo, R. Mexico and the COVID-19 Response. *Disaster Med. Public Health Prep.* **2020**, *14*, E17–E18. [CrossRef] [PubMed]
5. SINAVE. Gobierno de México. 2021. Available online: https://covid19.sinave.gob.mx/ (accessed on 14 September 2021).
6. Asadi, S.; Bouvier, N.; Wexler, A.S.; Ristenpart, W.D. The coronavirus pandemic and aerosols: Does COVID-19 transmit via expiratory particles? *Aerosol Sci. Technol.* **2020**, *54*, 635–638. [CrossRef]
7. Van Doremalen, N.; Bushmaker, T.; Morris, D.; Holbrook, M.; Gamble, A.; Williamson, B.; Tamin, A.; Harcourt, J.; Thornburg, N.; Gerber, S.; et al. Aerosol and surface stability of HCoV-19 (SARS-CoV-2) compared to SARS-CoV-1. *N. Engl. J. Med.* **2020**, *382*, 1564–1567. [CrossRef] [PubMed]
8. Bourouiba, L.; Dehandschoewercker, E.; Bush, J. Violent expiratory events: On coughing and sneezing. *J. Fluid Mech.* **2014**, *745*, 537–563. [CrossRef]
9. Xie, X.; Li, Y.; Chwang, A.T.Y.; Ho, P.L.; Seto, W.H. How far droplets can move in indoor environments—Revisiting the Wells evaporation–falling curve. *Indoor Air* **2007**, *17*, 211–225. [CrossRef] [PubMed]
10. Gupta, J.K.; Lin, C.H.; Chen, Q. Flow dynamics and characterization of a cough. *Indoor Air* **2009**, *19*, 517–525. [CrossRef]
11. Pavilonis, B.; Ierardi, A.M.; Levine, L.; Mirer, F.; Kelvin, E.A. Estimating aerosol transmission risk of SARS-CoV-2 in New York City public schools during reopening. *Environ. Res.* **2021**, *195*, 110805. [CrossRef]
12. Sun, C.; Zhai, Z. The efficacy of social distance and ventilation effectiveness in preventing COVID-19 transmission. *Sustain. Cities Soc.* **2020**, *62*, 102390. [CrossRef]
13. Bjørn, E.; Nielsen, P.V. Dispersal of exhaled air and personal exposure in displacement ventilated rooms. *Indoor Air* **2002**, *12*, 147–164. [CrossRef] [PubMed]
14. Beesoon, S.; Behary, N.; Perwuelz, A. Universal masking during COVID-19 pandemic: Can textile engineering help public health? Narrative review of the evidence. *Prev. Med.* **2020**, *139*, 106236. [CrossRef] [PubMed]
15. Atangana, E.; Atangana, A. Facemasks simple but powerful weapons to protect against COVID-19 spread: Can they have sides effects? *Results Phys.* **2020**, *19*, 103425. [CrossRef] [PubMed]
16. Xi, J.; Si, X.A.; Nagarajan, R. Effects of mask-wearing on the inhalability and deposition of airborne SARS-CoV-2 aerosols in human upper airway. *Phys. Fluids* **2020**, *32*, 123312. [CrossRef]
17. Leonard, S.; Strasser, W.; Whittle, J.; Volakis, L.; DeBellis, R.; Prichard, R.; Atwood, C.; Dungan, G. Reducing aerosol dispersion by high flow therapy in COVID-19: High resolution computational fluid dynamics simulations of particle behavior during high velocity nasal insufflation with a simple surgical mask. *J. Am. Coll. Emerg. Physicians Open* **2020**, *1*, 578–591. [CrossRef]
18. Tello-Leal, E.; Macías-Hernández, B.A. Association of environmental and meteorological factors on the spread of COVID-19 in Victoria, Mexico, and air quality during the lockdown. *Environ. Res.* **2021**, *196*, 110442. [CrossRef]
19. López-Feldman, A.; Heres, D.; Marquez-Padilla, F. Air pollution exposure and COVID-19: A look at mortality in Mexico City using individual-level data. *Sci. Total Environ.* **2021**, *756*, 143929. [CrossRef]
20. Morawska, L.; Johnson, G.R.; Ristovski, Z.D.; Hargreaves, M.; Mengersen, K.; Corbett, S.; Chao, C.Y.H.; Li, Y.; Katoshevski, D. Size distribution and sites of origin of droplets expelled from the human respiratory tract during expiratory activities. *J. Aerosol Sci.* **2009**, *40*, 256–269. [CrossRef]
21. Pendar, M.-R.; Páscoa, J.C. Numerical modeling of the distribution of virus carrying saliva droplets during sneeze and cough. *Phys. Fluids* **2020**, *32*, 083305. [CrossRef]
22. Mittal, R.; Ni, R.; Seo, J. The flow physics of COVID-19. *J. Fluid Mech.* **2020**, *894*, F2. [CrossRef]
23. Li, Y.; Wong, T.; Chung, J.; Guo, Y.P.; Hu, J.Y.; Guan, Y.T.; Yao, L.; Song, Q.W.; Newton, E. In vivo protective performance of N95 respirator and surgical facemask. *Am. J. Ind. Med.* **2006**, *49*, 1056–1065. [CrossRef] [PubMed]
24. Whiley, H.; Keerthirathne, T.P.; Nisar, M.A.; White, M.; Ross, K.E. Viral Filtration Efficiency of Fabric Masks Compared with Surgical and N95 Masks. *Pathogens* **2020**, *9*, 762. [CrossRef] [PubMed]

25. Dbouk, T.; Drikakis, D. On respiratory droplets and face masks. *Phys. Fluids* **2020**, *32*, 063303. [CrossRef]
26. Lei, Z.; Yang, J.; Zhuang, Z.; Roberge, R. Simulation and evaluation of respirator faceseal leaks using computational fluid dynamics and infrared imaging. *Ann. Occup. Hyg.* **2013**, *57*, 493–506. [CrossRef] [PubMed]
27. Verma, S.; Dhanak, M.; Frankenfield, J. Visualizing the effectiveness of face masks in obstructing respiratory jets. *Phys. Fluids* **2020**, *32*, 061708. [CrossRef]
28. Verma, S.; Dhanak, M.; Frankenfield, J. Visualizing droplet dispersal for face shields and masks with exhalation valves. *Phys. Fluids* **2020**, *32*, 091701. [CrossRef]
29. Martinez-Perez, C.; Monteiro, B.; Soares, M.; Portugues, F.; Matos, S.; Ferreira, A.; Alvarez-Peregrina, C.; Sánchez-Tena, M.Á. Influence of Face Masks on the Use of Contact Lenses. *Int. J. Environ. Res. Public Health* **2021**, *18*, 7407. [CrossRef]
30. Khosronejad, A.; Santoni, C.; Flora, K.; Zhang, Z.; Kang, S.; Payabvash, S.; Sotiropoulos, F. Fluid dynamics simulations show that facial masks can suppress the spread of COVID-19 in indoor environments. *AIP Adv.* **2020**, *10*, 125109. [CrossRef]
31. Cornejo, P.; Guerrero, N.; Sandoval, V. Aerodynamic Dispersion of Respiratory Droplets and Aerosols by Turbulent Airflow. *Fluids* **2021**, *6*, 119. [CrossRef]
32. Peric, R.; Perić, M. Analytical and numerical investigation of the airflow in face masks used for protection against COVID-19 virus implications for mask design and usage. *J. Appl. Fluid Dyn.* **2020**, *13*, 1911–1923. [CrossRef]
33. Tino, R.; Moore, R.; Antoline, S.; Ravi, P.; Wake, N.; Ionita, C.N.; Morris, J.M.; Decker, S.J.; Sheikh, A.; Rybicki, F.J.; et al. COVID-19 and the role of 3D printing in medicine. *3D Print. Med.* **2020**, *6*, 11. [CrossRef] [PubMed]
34. Tcharkhtchi, A.; Abbasnezhad, N.; Seydani, M.Z.; Zirak, N.; Farzaneh, S.; Shirinbayan, M. An overview of filtration efficiency through the masks: Mechanisms of the aerosols penetration. *Bioact. Mater.* **2021**, *6*, 106–122. [CrossRef]
35. Tu, J.; Yeoh, G.-H.; Liu, C. Chapter 3—Governing Equations for CFD. In *Computational Fluid Dynamics*, 2nd ed.; Butterworth-Heinemann: Oxford, UK, 2013; pp. 61–121. ISBN 9780080982434. Available online: https://www.sciencedirect.com/science/article/pii/B9780080982434000032 (accessed on 14 September 2021). [CrossRef]
36. Chung, T.J. *Computational Fluid Dynamics*, 2nd ed.; Cambridge University Press: Cambridge, UK, 2014; p. 1058. ISBN 1107425255.
37. Launder, B.E.; Spalding, D.B. The numerical computation of turbulent flows. *Comput. Methods Appl. Mech. Eng.* **1974**, *3*, 269–289. [CrossRef]
38. ANSYS FLUENT, Inc. User's Guide 12.0. 2009. Available online: https://www.afs.enea.it/project/neptunius/docs/fluent/html/ug/main_pre.htm (accessed on 14 September 2021).
39. Villanueva-Bonilla, S.; Saavedra-Layera, L.; Vergara-Núñez, C. Comparación de mediciones antropométricas directa y con sistema de imagen 3D, en adultos jóvenes. *Rev. Clínica Periodoncia Implantol. Rehabil. Oral* **2018**, *11*, 16–19. [CrossRef]
40. Tsega, E.G. Computational Fluid Dynamics Modeling of Respiratory Airflow in Tracheobronchial Airways of Infant, Child, and Adult. *Comput. Math. Methods Med.* **2018**, *2018*, 9603451. [CrossRef]
41. Russo, J.S.; Khalifa, E. Computational study of breathing methods for inhalation exposure. *HVACR Res.* **2011**, *17*, 419–431. [CrossRef]
42. Eshbaugh, J.P.; Gardner, P.D.; Richardson, A.W.; Hofacre, K.C. N95 and P100 Respirator Filter Efficiency Under High Constant and Cyclic Flow. *J. Occup. Environ. Hyg.* **2008**, *6*, 52–61. [CrossRef]
43. Gupta, J.K.; Lin, C.H.; Chen, Q. Characterizing exhaled airflow from breathing and talking. *Indoor Air* **2010**, *20*, 31–39. [CrossRef]
44. Flora, J.R.V.; Hargis, R.A.; O'Dowd, W.J.; Karash, A.; Pennline, H.W.; Vidic, R.D. The Role of Pressure Drop and Flow Redistribution on Modeling Mercury Control Using Sorbent Injection in Baghouse Filters. *J. Air Waste Manag. Assoc.* **2006**, *56*, 343–349. [CrossRef]
45. Jobic, Y.; Kumar, P.; Topin, F.; Occelli, R. Determining permeability tensors of porous media: A novel 'vector kinetic' numerical approach. *Int. J. Multiph. Flow* **2019**, *110*, 198–217. [CrossRef]
46. Eninger, R.M.; Honda, T.; Adhikari, A.; Heinonen-Tanski, H.; Reponen, T.; Grinshpun, S.A. Filter Performance of N99 and N95 Facepiece Respirators against Viruses and Ultrafine Particles. *Ann. Occup. Hyg.* **2008**, *52*, 385–396. [CrossRef] [PubMed]
47. Gao, P.; Jaques, P.A.; Hsiao, T.-C.; Shepherd, A.; Eimer, B.C.; Yang, M.; Miller, A.; Gupta, B.; Shaffer, R. Evaluation of Nano- and Submicron Particle Penetration through Ten Nonwoven Fabrics Using a Wind-Driven Approach. *J. Occup. Environ. Hyg.* **2011**, *8*, 13–22. [CrossRef] [PubMed]
48. Betsch, C.; Korn, L.; Sprengholz, P.; Felgendreff, L.; Eitze, S.; Schmid, P.; Böhm, R. Social and behavioral consequences of mask policies during the COVID-19 pandemic. *Proc. Natl. Acad. Sci. USA* **2020**, *117*, 21851–21853. [CrossRef] [PubMed]